

Pharmacokinetics, Mass Balance, and Metabolism of the Novel Urate Transporter 1 Inhibitor [^{14}C]HR011303 in Humans: Metabolism Is Mediated Predominantly by UDP-Glucuronosyltransferase

Yuandong Zheng, Hua Zhang, Mengling Liu, Guangze Li, Sheng Ma, Zhe Zhang, Hongda Lin, Yan Zhan, Zhendong Chen, Dafang Zhong, Liyan Miao, and Xingxing Diao

Shanghai Center for Drug Metabolism and Pharmacokinetics, Shanghai Institute of Materia Medica, Chinese Academy of Sciences, Shanghai, China (Y.Zhe., M.L., Y.Zha., Z.C., D.Z., X.D.); University of Chinese Academy of Sciences, Beijing, China (Y.Zhe., M.L., Y.Zha., Z.C., D.Z., X.D.); Department of Clinical Pharmacology, the First Affiliated Hospital of Soochow University, Suzhou, China (H.Z., S.M., L.M.); Institute for Interdisciplinary Drug Research and Translational Sciences, Soochow University, Suzhou, China (H.Z., S.M., L.M.); and Jiangsu Hengrui Medicine Co., Ltd., Shanghai, China (G.L., Z.Z., H.L.)

Received June 14, 2021; accepted November 30, 2021

ABSTRACT

HR011303, a promising selective urate transporter 1 inhibitor, is currently being studied in a phase III clinical trial in China for the treatment of hyperuricemia and gout. In the current study, the pharmacokinetics, mass balance, and metabolism of HR011303 were examined in six healthy Chinese male subjects who received a single oral dose of 10 mg of [^{14}C]HR011303 (80 μCi). The results showed that HR011303 was rapidly absorbed with a median time to reach C_{max} of 1.50 hours postdose, and the arithmetic mean half-life of total radioactivity was approximately 24.2 hours in plasma. The mean blood-to-plasma radioactivity concentration ratio was 0.66, suggesting the preferential distribution of drug-related components in plasma. At 216 hours postdose, the mean cumulative excreted radioactivity was 91.75% of the dose, including 81.50% in urine and 10.26% in feces. Six metabolites were identified, and the parent drug HR011303 was the most abundant component in plasma and feces, but a minor component in urine. Glucuronidation of the

carboxylic acid moiety of HR011303 was the primary metabolic pathway in humans, amounting to 69.63% of the dose (M5, 51.57% of the dose; M5/2, 18.06% of the dose) in the urine; however, it was not detected in plasma. UDP-glucuronosyltransferase (UGT) 2B7 was responsible for the formation of M5. Overall, after a single oral dose of 10 mg of [^{14}C]HR011303 (80 μCi), HR011303 and its main metabolites were eliminated via renal excretion. The major metabolic pathway was carboxylic acid glucuronidation, which was catalyzed predominantly by UGT2B7.

SIGNIFICANCE STATEMENT

This study determined the absorption and disposition of HR011303, a selective urate transporter (URAT) 1 inhibitor currently in development for the treatment of hyperuricemia and gout. This work helps to characterize the major metabolic pathways of new URAT inhibitors and identify the absorption and clearance mechanism.

Introduction

Hyperuricemia results from a high concentration of serum urate in the human body (Sui et al., 2008; Dong et al., 2019). According to the report “Prevalence of hyperuricemia among Chinese adults,” nearly 9.9% of men and 7% of women in China suffer from this illness (Liu et al., 2014). This condition is related to many chronic conditions, such

as gout and cardiovascular and renal diseases (Lee et al., 2012; Zoccali and Mallamaci, 2013; Gliozzi et al., 2016). As the most common clinical manifestation of hyperuricemia, gout is caused by the formation and deposition of monosodium urate crystals (Punzi et al., 2012; Tian et al., 2016) and may result in permanent joint destruction and kidney impairment, thereby dramatically affecting the quality of life of patients when left untreated or inadequately managed (Richette and Bardin, 2010).

With improvements in human quality of life and dietary habits, the concentration of urate in the human body has greatly increased; therefore, the global incidence of hyperuricemia and gout has gradually risen and the age of the patients has decreased (Liu et al., 2014; Kuo et al., 2015). Urate is metabolically degraded from purine nucleotides, nucleosides, and inosine, which are abundant in food. In most species, uricase easily converts urate into allantoin, which is 10 times more water-soluble, for elimination (Richette and Bardin, 2010; Burns and Wortmann, 2011). However, humans lack this enzyme (Tian et al., 2016). One-third of urate is excreted via the gastrointestinal tract and two-thirds via the

This study was sponsored by Jiangsu Hengrui Medicine Co., Ltd., and was partially supported by the National Natural Science Foundation of China [Grant 81903701] and the National Key New Drug Creation Special Programs [Grant 2017ZX09304-021].

G.Z.L., Z.Z., and H.D.L. are employees of Jiangsu Hengrui Medicine Co., Ltd. The other authors do not have an actual or perceived conflict of interest with the contents of this article.

Y.Zhe. and H.Z. contributed equally to this work.

dx.doi.org/10.1124/dmd.120.000581.

ABBREVIATIONS: AUC, area under the curve; AUC_{inf} , area under the curve from time 0 to infinity; CL_{int} , intrinsic clearance; CMC-Na, carboxymethyl cellulose sodium; FA, formic acid; HKM, human kidney microsome; HLM, human liver microsome; IS, internal standard; K_m , Michaelis-Menten constant; LC-MS/MS, liquid chromatography-tandem mass spectrometry; MS, mass spectrometry; $t_{1/2}$, half-life; UDPGA, uridine 5'-diphosphoglucuronic acid; UGT, UDP-glucuronosyltransferase; UHPLC, ultra-high performance liquid chromatography; URAT, urate transporter; XO, xanthine oxidase inhibitor.

kidney; however, 90% of the urate filtered by the kidney is reabsorbed by the body (Hyndman et al., 2016; Maiuolo et al., 2016). Among patients with hyperuricemia and gout, 90% have impaired renal urate excretion and 10% are overproducers (Punzi et al., 2012). Therefore, drug candidates must be developed to reduce urate levels in the human body.

The currently available drugs for the clinical treatment of hyperuricemia and gout can be roughly classified into three groups. One group is uric acid decomposition drugs, such as rasburicase and pegloticase; however, their utilization is restricted by severe side effects and high cost (Lipsky et al., 2014). The second group is xanthine oxidase inhibitors (XOIs), which inhibit the conversion of xanthine into uric acid. Although XOIs show advantages to treat hyperuricemia and gout, their side effects, such as severe allergic reactions, diarrhea, and drowsiness, cannot be ignored (Pacher et al., 2006; Jordan and Gresser, 2018). The third group is uricosuric agents, and the representative drugs of this group are the highly selective urate transporter (URAT) 1 inhibitors. URAT1 inhibitors are usually employed to interrupt the reabsorption of uric acid that has been filtered by the kidney (Hediger et al., 2005; Sakiyama et al., 2016). URAT1 is prominently expressed in the epithelial cells of the proximal tubules in the renal cortex and has become a research hotspot (Kuo et al., 2017; Dong et al., 2019; Novikov et al., 2019). However, the current clinically available URAT1 inhibitors are limited because of their severe adverse reactions. For example, lesinurad, the most commonly used URAT1 inhibitor in the clinic, was approved for use only in combination with a XO inhibitor for the treatment of hyperuricemia and gout (Hoy, 2016). Hence, novel URAT1 inhibitors to control urate levels in patients are urgently needed.

HR011303 is a drug candidate developed by Jiangsu Hengrui Medicine Co., Ltd., and it is currently undergoing phase III clinical trials in China for the treatment of hyperuricemia and gout (Peng et al., 2016). Previous studies have shown that HR011303 substantially decreases serum urate levels (Dong et al., 2019). Preclinical pharmacology studies revealed that HR011303 is a potent and selective URAT1 inhibitor and holds great potential for the treatment of the above diseases (Peng et al., 2016; Wang et al., 2019).

Although HR011303 shows potential as a first-line medicine, its human metabolite profile and pharmacokinetic properties have not yet been reported. In this study, [^{14}C]HR011303 was administered to healthy Chinese male subjects to (1) investigate the pharmacokinetics, mass balance, and biotransformation of HR011303 in humans; (2) quantify the predominant drug-related components in human plasma; and (3) identify the enzymes responsible for HR011303 glucuronidation by using human liver microsomes (HLMs), human kidney microsomes (HKMs), and recombinant UDP-glucuronosyltransferases (UGTs).

Materials and Methods

Chemicals and Reagents

HR011303 (chemical purity, 98.40%), [^{14}C]HR011303 (chemical purity, 98.77%; specific activity, 58.0 mCi/mmol; radiochemical purity, 99.08%), M5 (chemical purity, 95.40%), and internal standard (IS) SHR144764 (chemical purity, 98.20%) were supplied by Jiangsu Hengrui Medicine Co., Ltd. (Shanghai, China). Ammonium acetate and formic acid (FA) were supplied by Sinopharm Chemical Reagent Co., Ltd. (Shanghai, China) and Rhawn Chemical Reagent Co., Ltd. (Shanghai, China), respectively. Niflumic acid, fluconazole, carboxymethyl cellulose sodium (CMC-Na), uridine 5'-diphosphoglucuronic acid (UDPGA), alamechicin, phosphate buffer saline (PBS), and Tris-HCl were purchased from Meilunbio (Dalian, China). A mixed gender pool of 150 HLMs and recombinant UGTs were supplied by Corning Gentest (Woburn, MA), and a mixed gender pool of eight HKMs was supplied by Sekisui Xenotech (Kansas City, KS). A Milli-Q integral water purification system (Millipore, Molsheim, France) was used to produce ultrapure water, and high performance liquid chromatography-grade acetonitrile and methanol were purchased from Sigma (St. Louis, MO). All other chemicals were of analytical grade.

In brief, 5.77 mg of [^{14}C]HR011303 sodium salt (approximately 800 μCi) was dissolved in 480 mL of 0.5% CMC-Na (US Pharmacopeia grade) solution and then equally aliquoted into 10 bottles with each bottle containing 80 μCi of [^{14}C]HR011303. Next, a 10 mg HR011303 tablet was ground and suspended in 20 mL of 0.5% CMC-Na solution, and the suspension was transferred to each bottle containing [^{14}C]HR011303 suspensions. The volume of the resulting suspensions was adjusted to 80 mL with 0.5% CMC-Na solution. Before the day of administration, the prepared oral suspension was preserved at approximately -80°C . The ^{14}C was labeled on the benzene ring as shown in Fig. 1.

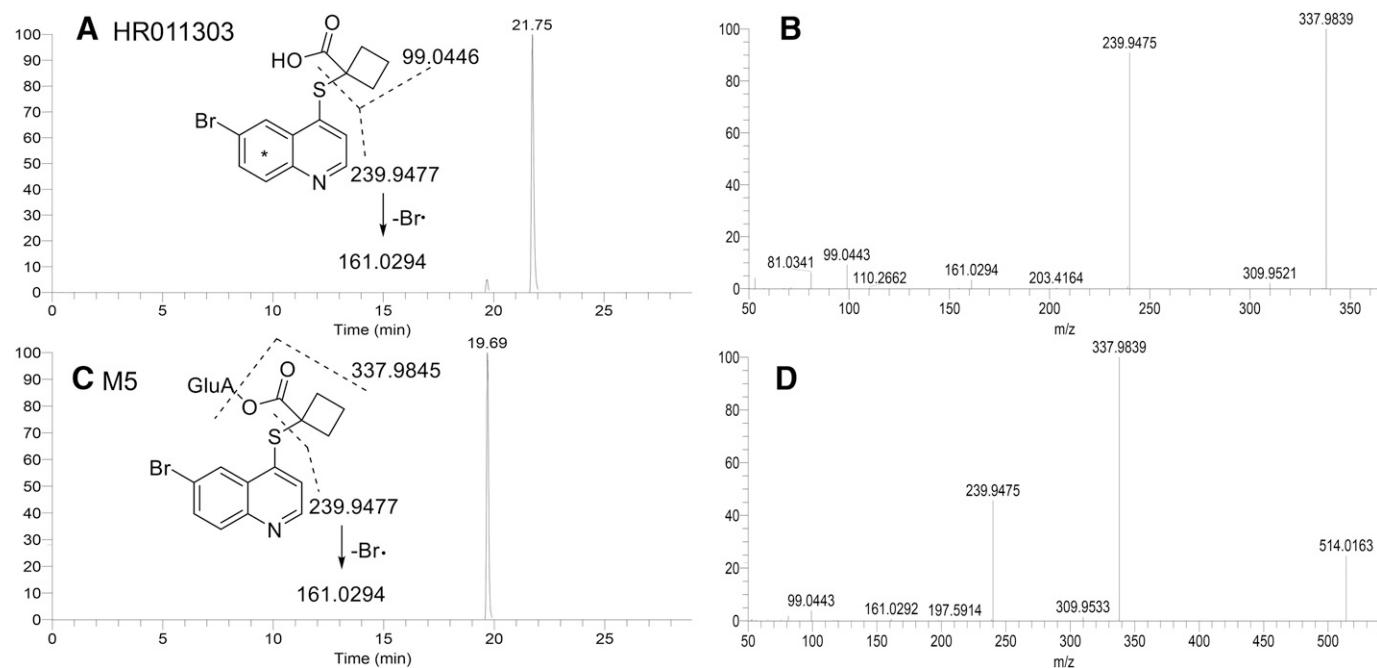


Fig. 1. Extracted ion chromatograms, product ion spectra, and proposed fragmentation patterns of HR011303 (A, B) and M5 (C, D). * indicates ^{14}C labeled position.

Instruments and Conditions

The instruments, parameters for the high-resolution mass spectrometry mass conditions, and data acquisition and analyses were the same as those previously described (Zheng et al., 2021). Separation of the analytes was achieved with an HSS T₃ C₁₈ column (100 × 2.1 mm, 1.8 μm; Waters, Milford, MA) at 40°C. The mobile phase, consisting of 5 mM ammonium acetate in water with 0.05% FA (A) and acetonitrile (B), was delivered at a constant flow rate of 0.5 mL/min. The gradient elution program was as follows: 0.0 minutes, 5% B; 3.0 minutes, 5% B; 24.0 minutes, 40% B; 26.0 minutes, 95% B; 28.8 minutes, 95% B; 28.9 minutes, 5% B; and 35.0 minutes, 5% B.

Study Subjects and Sample Collection

This open-label, single-center, single-dose study was conducted in six healthy Chinese male subjects (ages 24–34 with body mass indexes of 21.2–25.2 kg/m²) at the First Affiliated Hospital of Soochow University (Suzhou, China) in accordance with the Declaration of Helsinki. All participants provided written informed consent, and all study-relevant materials were approved by the Hospital Ethics Committee. Plasma, urine, and fecal samples were collected 0–216 hours after oral administration. The discharge criteria were the same as those from a previous report (Bian et al., 2020; Zheng et al., 2021). Each of the six subjects received a single oral dose of 10 mg of [¹⁴C]HR011303 (80 μCi) as a suspension after fasting for at least 10 hours. The bottle used for administration was rinsed with pure water, and the volunteers consumed the rinse fluids within 10 minutes (the total consumed fluid was approximately 240 mL). The subjects were forbidden to drink water for 1 hour and fasted for 4 hours after taking the drug. Eleven mL of whole blood was collected at predose and 1, 2, 4, 12, 24, and 48 hours postdose. From these samples, 1 mL of blood was aliquoted into two vials (0.5 mL for each vial) and the remaining blood (10 mL) was centrifuged to yield plasma. Afterward, 3.2 mL and 0.8 mL of plasma were immediately mixed with 160 μL and 40 μL protease inhibitor cocktail, respectively, in an ice-water bath. At 0.25, 0.5, 1.5, 3, 6, 8, 10, 72, 96, 120, 144, 168, 192, and 216 hours postdose, 4 mL of whole blood was collected and centrifuged to yield plasma. Afterward, 1.2 mL and 0.4 mL of plasma were immediately mixed with 60 μL and 20 μL protease inhibitor cocktail, respectively, in an ice-water bath. Whole blood and plasma samples were preserved at approximately –80°C until analysis. Urine samples were collected at predose and for 0–4, 4–8, 8–12, and 12–24 hours postdose and every 24 hours thereafter until 216 hours. Feces samples were collected at predose and every 24 hours thereafter until 216 hours. The urine and fecal samples were preserved at approximately –20°C until analysis.

Total Radioactivity Analysis

A liquid scintillation counter (TriCarb 3110TR, PerkinElmer, Waltham, MA) was used to measure the total radioactivity in the plasma and urine. Each fecal sample was mixed with acetonitrile–water (1:1, v:v) at twice the weight of feces, and then homogenized. Blood and fecal homogenates were aliquoted and combusted using an OX-501 Biologic Oxidizer (Harvey, Tappan, NY), and the product of combustion, trapped as ¹⁴CO₂, was mixed with alkaline RDC scintillation fluid (RDC, Hillsdale, NJ) and measured using a liquid scintillation counter.

Sample Preparation for Metabolic Radio-Profiling

Plasma. Plasma (6.0 mL) was pooled from the six subjects according to the Hamilton pooling principle (Hop et al., 1998). A 4.5 mL aliquot of plasma was treated according to the same method as that described in a previous study to obtain 380 μL of reconstitution solution (Zheng et al., 2021). Sixty microlitre of plasma reconstitution solution was injected into an ultra-high performance liquid chromatography (UHPLC) Fraction Collector (Thermo) to obtain the eluent, which was then collected in Deepwell LumaPlate 96-well plates (PerkinElmer) for the first 29 minutes with every 10-second fraction and chant into one to per well. A Sense Beta plate reader (Hidex, Turku, Finland) was used to measure the radioactivity values of each well after the plates were dried at room temperature in the airing chamber overnight. Subsequently, the data obtained from the Sense Beta were reconstructed into a radio-chromatogram by Laura software (LabLogic, Broomhill, Sheffield, United Kingdom). In addition, 10 μL of reconstitution solution was used for mass spectrometry (MS) analysis.

Urine and Feces. The methods of pooling urine for 0–48 hours and feces for 0–72 hours from the six subjects, as well as sample preparation to obtain the corresponding reconstitution solutions (urine, 550 μL; feces, 200 μL), were the same as those in a published article (Zheng et al., 2021). Ten microlitre of urine

reconstitution was used for radio-profiling in β-RAM (LabLogic), and 5 μL of reconstitution solution was used for MS analysis. Moreover, 40 μL of fecal reconstitution solution was used for radio-profiling using the same method as that for plasma, and 7 μL of reconstitution solution was used for MS analysis.

The recovery from the plasma, urine, and fecal samples after each step of preparation was greater than 90%.

Metabolite Identification

Mass spectral fragmentations of the parent compound (HR011303) and reference substance (the glucuronide metabolite, M5) were used to identify the metabolite structures via UHPLC-Q Exactive Plus MS. The bromine isotopic distribution pattern was also used for metabolite identification. Metabolites with a bromine atom display [M + H]⁺/[M + H + 2]⁺ isotopes in their full mass spectrum with a relative abundance of approximately 1:1 aided in the identification of metabolites.

Determination of Glucuronide Metabolite M5 in Human Plasma

Plasma samples pretreated with protease inhibitor cocktail were used to determine the concentrations of HR011303 and M5. The pretreated plasma was spiked with IS working solution and vortexed, and then acetonitrile was added for protein precipitation. HR011303, M5, and IS were separated on an HSS T₃ column (50 × 2.1 mm, 1.8 μm; Waters) with the temperature maintained at 40°C. The mobile phase consisted of water with 0.3% FA and acetonitrile at a flow rate of 0.6 mL/min. HR011303 and M5 were quantitated on a 6500 triple quadrupole mass spectrometer (Sciex, Framingham, MA) coupled with an LC-30AD high performance liquid chromatography system (Shimadzu, Kyoto, Japan). The quantitative transition ion pairs were *m/z* 338.1→240.0 (HR011303), *m/z* 514.1→338.2 (M5), and *m/z* 328.1→230.0 (IS). Data acquisition and processing were conducted using Analyst 1.6.2 software (Sciex). The calibration curves were linear over the plasma concentration ranges of 10.0–10,000 and 0.500–500 ng/mL for HR011303 and M5, respectively. The lower limits of quantification for HR011303 and M5 were 10.0 and 0.500 ng/mL, respectively.

Pharmacokinetics Analysis

The definitions and calculations of the pharmacokinetic parameters, blood-to-plasma ratio, area under the curve (AUC) ratio of the parent and metabolites to total radioactivity, and radioactivity excretion in urine and feces (percentage of dose) were the same as those in an earlier report (Zheng et al., 2021).

In Vitro Incubations with UGTs

HR011303 was dissolved in methanol–water (1:1, v:v), and alamethicin was dissolved in dimethyl sulfoxide (DMSO). Both stock solutions were serially diluted with 50 mM Tris-HCl buffer (pH 7.5) to the desired concentrations. A typical incubation system (200 μL of total volume) contained 50 mM Tris-HCl buffer, 8 mM MgCl₂, 25 μg/mL alamethicin, and 10 μM HR011303 with 1 of 13 commercially available recombinant UGT enzymes, namely, UGT1A1, UGT1A3, UGT1A4, UGT1A5, UGT1A7, UGT1A8, UGT1A9, UGT1A10, UGT2B4, UGT2B7, UGT2B10, UGT2B15, or UGT2B17. The final concentration of each recombinant enzyme was 0.5 mg protein/mL. After preincubation at 37°C for 3 minutes, the reactions were initiated by the addition of UDPGA dissolved in Tris-HCl buffer. The final UDPGA concentration was 2 mM. The reactions were maintained at 37°C for 1 hour and terminated with an equal volume of ice-cold acetonitrile containing 50 ng/mL IS. Incubations in the absence of a recombinant UGT served as the negative control. Each incubation was conducted in duplicate.

In Vitro Incubations of HR011303 in Pooled HLMs and HKMs

HLMs and HKMs were used to identify the UGTs that participate in M5 formation. The assay conditions were the same as those for the incubation of HR011303 with recombinant UGTs with one exception: 1 mg/mL HLMs or 1 mg/mL HKMs were used instead of 0.5 mg/mL recombinant UGT protein.

Different chemical inhibitors were used to determine their effects. Niflumic acid is a specific inhibitor of UGT1A9, and fluconazole is an inhibitor of UGT2B7. Fluconazole also shows an inhibitory effect on UGT2B4 at high concentrations (Al Saabi et al., 2013; Ramirez et al., 2015). Niflumic acid and fluconazole were dissolved in DMSO as stock solutions, and both stock solutions were diluted with 50 mM Tris-HCl buffer (pH 7.5) to the desired concentrations.

The other assay conditions were the same as those described above. Incubations without inhibitor were normalized to 100%.

Stability Studies of M5 in PBS, Plasma, and Urine

A stock solution of M5 (10 mM) was diluted to 50 μ M with PBS. The incubation mixtures (100 μ L of total volume) consisted of 10 μ L of M5 solution and 90 μ L of PBS, human plasma (5% volume of cocktail inhibitor or DMSO), or human urine. M5 was incubated for the designed time and terminated with the addition of 1000 μ L of ice-cold acetonitrile (0.1% FA, IS: 100 ng/mL). Each incubation was conducted in duplicate, and then the M5 concentration was quantified using liquid chromatography-tandem mass spectrometry (LC-MS/MS).

Enzyme Kinetics Studies

Kinetics studies for UGT2B4 and UGT2B7 were conducted with recombinant UGT2B4 and UGT2B7 using a protein concentration of 0.25 mg/mL. The ranges of HR011303 concentrations used to obtain kinetics profiles were 0.1 to 100 μ M, and the incubation time was 30 minutes for UGT2B4, whereas the incubation time for UGT2B7 was 15 minutes. For the kinetics studies, the formation rates of M5 were linear with respect to both UGTs concentration and incubation time.

Enzyme Kinetics Data Analysis

The obtained data were used to draw Eadie-Hofstee curves, which contributed to the evaluation of the kinetics models (Hutzler and Tracy, 2002). The kinetics parameters were acquired by fitting the velocity data to appropriate kinetics models (1 and 2) using GraphPad Prism 8.0 software (GraphPad Software Inc., San Diego, CA).

When the data fit the biphasic kinetics model, eq. 1 was applied (Leow and Chan, 2019):

$$v = V_{max1} \times [S]/(K_{m1} + [S]) + V_{max2} \times [S]/(K_{m2} + [S]) \quad (1)$$

where v , V_{max} , $[S]$, and K_m are the rate of reaction, maximum velocity, substrate concentration, and Michaelis-Menten constant, respectively. In addition, K_{m1} represents the high-affinity component, and K_{m2} represents the low-affinity component ($K_{m1} < K_{m2}$).

Equation 2 was used when the data fit the substrate inhibition kinetics model (Leow and Chan, 2019).

$$v = V_{max}/(1 + K_m/[S]) + [S]/(K_i) \quad (2)$$

where K_i represents the dissociation constant for the inhibitory substrate-enzyme-substrate complex.

Determination of Glucuronide Metabolite M5 in Vitro

In vitro samples were used to determine the M5 concentration. The analyte was separated on an HSS T3 column (50 \times 2.1 mm, 1.8 μ m, Waters) with the temperature maintained at 40°C. The mobile phase consisted of water with 0.3% FA (A) and acetonitrile (B) at the flow rate of 0.4 mL/min. M5 was quantitated on a 6495 triple quadrupole mass spectrometer coupled with 1290 infinity UHPLC system (Agilent, Santa Clara, CA). The quantitative transition ion pairs were m/z 514.1 \rightarrow 338.2 (M5) and m/z 328.1 \rightarrow 230.0 (IS).

Results

High Resolution Mass Spectrometry Analysis of HR011303 and M5

The fragmentation patterns of major product ions of HR011303 and M5 were characterized on the basis of accurate mass measurements to identify potential metabolites.

HR011303, $C_{14}H_{13}O_2NBrS$, with $[M+H]^+$ at m/z 337.9847, eluted at 21.75 minutes and showed product ions at m/z 81.0341, 99.0443, 161.0294, and 239.9475 (Fig. 1, A and B). The fragment ions at m/z 239.9475 and 99.0443 were generated by C-S cleavage, and m/z 161.0294 was produced by the further loss of a Br radical from m/z 239.9475.

M5, $C_{20}H_{21}O_8NBrS$, with $[M+H]^+$ at m/z 514.0171, eluted at 19.69 minutes and showed product ions at m/z 99.0443, 161.0292, 239.9475,

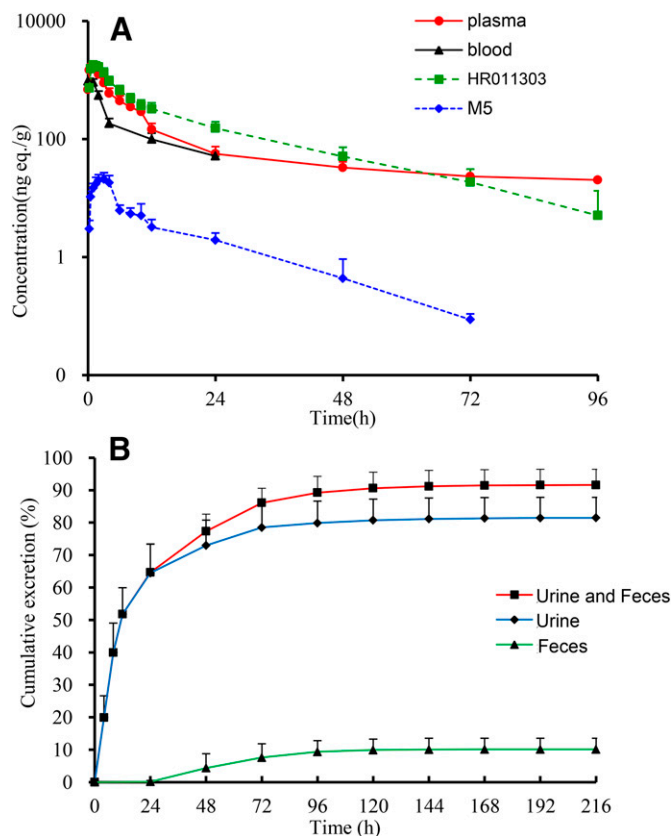


Fig. 2. Mean concentration of radioactivity in human blood and plasma and mean concentration of HR011303 and M5 in human plasma (A); mean cumulative excretion of total radioactivity in urine and feces after a single oral administration of [¹⁴C]HR011303 (B). Each point represents the mean \pm SD of six subjects.

and 337.9839 (Fig. 1, C and D). The fragment ion at m/z 337.9839 was generated from the neutral loss of glucuronic acid ($C_6H_8O_6$, -176.0324 Da). The other product ions were the same as those for HR011303.

Pharmacokinetics

Radio-pharmacokinetics. The total radioactivity concentration-time profiles in the blood and plasma after a single oral administration of 10 mg of [¹⁴C]HR011303 (80 μ Ci) to healthy Chinese male subjects are shown in Fig. 2A, and the related radioactive pharmacokinetic parameters are summarized in Table 1. In plasma, the geometric mean C_{max} of the total radioactivity was 1730 ng eq./mL, and the geometric mean, area under the curve from time 0 to infinity (AUC_{inf}) value was

TABLE 1

Pharmacokinetic parameters of total radioactivity, HR011303, and M5 in plasma after a single oral administration of [¹⁴C]HR011303 to healthy volunteers (mean (s.d. or cv%)) using noncompartmental methods in Phoenix WinNonlin

Parameter	Unit	¹⁴ C Plasma	HR011303	M5
C_{max}^a	ng eq./mL	1730 (12.0)	1840 (13.3)	20.5 (29.08)
AUC_{last}^a	ng (eq.)/mL·h	15200 (23.9)	15900 (22.8)	165 (38.8)
AUC_{inf}^a	ng (eq.)/mL·h	16100 (23.2)	16300 (22.4)	183 (35.7)
$t_{1/2}^b$	h	24.2 (10.3)	16.6 (3.85)	12.7 (4.93)
T_{max}^c	h	1.50 (33.5)	1.25 (42.0)	3.00 (36.9)

AUC_{last} , area under the curve from time 0 to the last measurable time point; T_{max} , time to reach C_{max} .

^aGeometric mean (cv%).

^bArithmetic mean (s.d.).

^cMedian mean (s.d.).

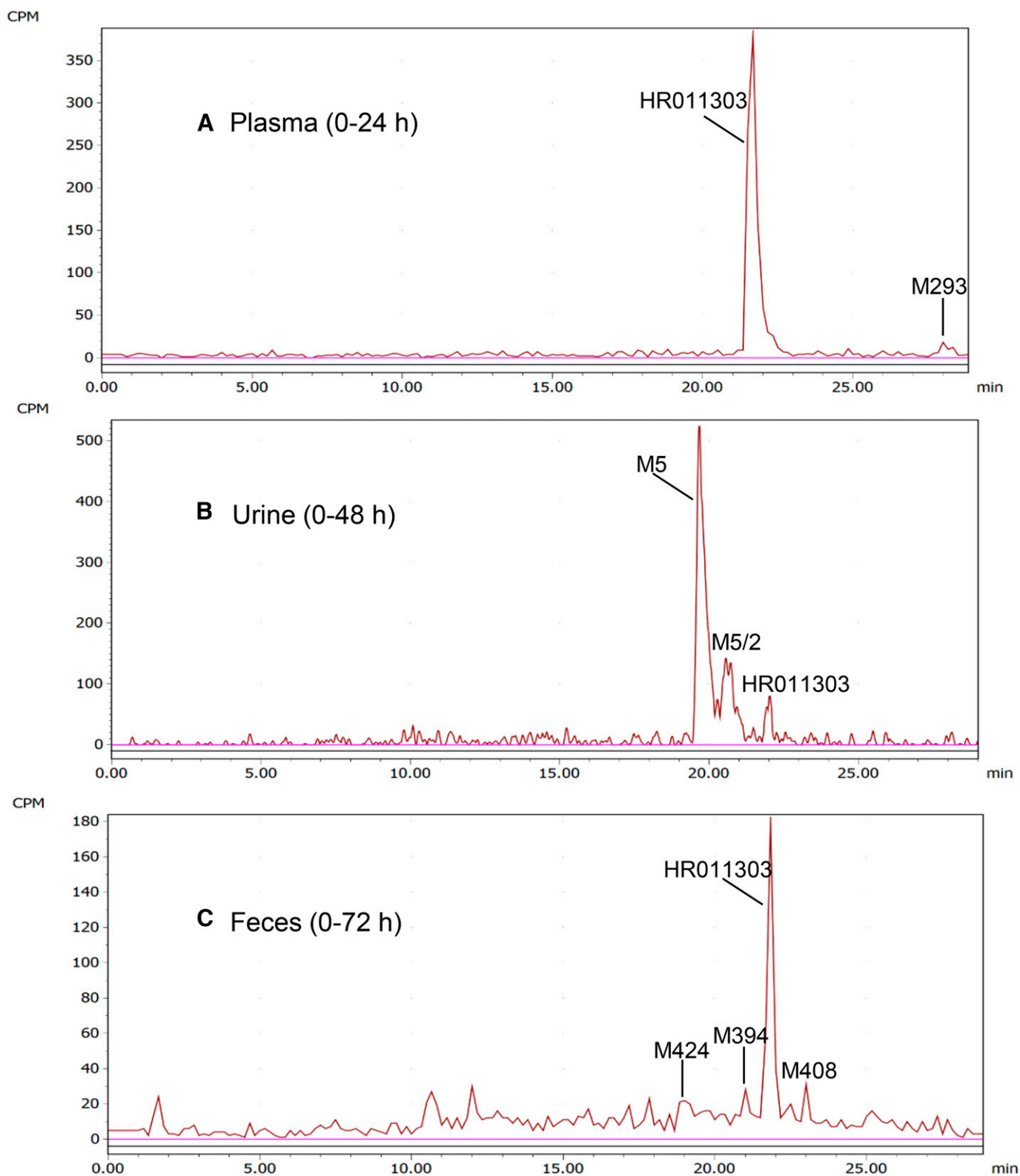


Fig. 3. Representative radio-chromatograms of the metabolites in human plasma (0–24 hours), urine (0–48 hours), and feces (0–72 hours) after oral administration of 10 mg of [^{14}C]HR011303 (80 μCi).

16,100 ng eq./mL·h. The median time to reach C_{max} of plasma was approximately 1.50 hours, and the arithmetic mean half-life ($t_{1/2}$) was approximately 24.2 hours. The blood-to-plasma ratio of the radioactivity was 0.66.

LC-MS/MS quantification of HR011303 and M5 in plasma. The mean plasma concentration–time curves of HR011303 and M5 are shown in Fig. 2A, and their pharmacokinetic parameters are presented in Table 1. The arithmetic mean $t_{1/2}$ was 16.6 hours for HR011303 and

TABLE 2

Information on HR011303 metabolites detected in human plasma, urine, and feces by using UHPLC-Q Exactive Plus MS

ID	Metabolic Pathway	Formula	[M+H] ⁺ <i>m/z</i> Measured	Mass Error (ppm)	Fragment Ions
HR011303	Parent	C ₁₄ H ₁₂ O ₂ NBrS	337.9844	−0.2	337.9839, 309.9521, 239.9475, 161.0294, 99.0443
M5	[GluA]	C ₂₀ H ₂₀ O ₈ NBrS	514.0165	−0.1	514.0163, 337.9839, 309.9533, 239.9475, 161.0292, 99.0442
M5/2	[GluA]	C ₂₀ H ₂₀ O ₈ NBrS	514.0165	−1.1	514.0155, 337.9839, 319.9731, 239.9475, 99.0422
M293	−COOH	C ₁₃ H ₁₂ NBrS	293.9944	−0.9	293.9939, 239.9475, 161.0291
M394	−H ₂ O+[Gly]	C ₁₆ H ₁₅ O ₃ N ₂ BrS	395.0062	0.6	395.0050, 319.9731, 239.9472, 156.0653, 110.0603
M408	−H ₂ O+[Ala]	C ₁₇ H ₁₇ O ₃ N ₂ BrS	409.0220	1.0	409.0204, 319.9734, 239.9471, 170.0809, 124.0755
M424	M408+[O]	C ₁₇ H ₁₇ O ₄ N ₂ BrS	425.0165	0.5	425.0156, 319.9729, 239.9473, 186.0757, 140.0703

[Ala], alanine; [GluA], glucuronidation; [Gly], glycine; [O], oxidation.

12.7 hours for M5. The geometric mean C_{\max} was 1840 ng/mL for HR011303 and 20.5 ng/mL for M5. The geometric mean exposure (AUC_{inf}) was 16,300 ng/mL·h for HR011303 and 183 ng/mL·h for M5. According to the AUC_{inf} ratios, HR011303 was the most abundant drug-related component, accounting for 101.26%, and M5 was a minor component constituting 1.16% of the total radioactivity in plasma.

Mass Balance

For the six healthy Chinese male subjects who received 10 mg of [¹⁴C]HR011303 (80 μCi) orally, the mean total radioactivity recovery was 91.75% (range 86.94%–96.56%) after 216 hours. Urine excretion was the predominant route of elimination constituting 81.50% of the administered dose, and fecal excretion accounted for 10.26%. The total recovery of radioactivity in the urine and feces from 0–96 hours after dosing was 89.40%, as shown in Fig. 2A.

Metabolite Profiling and Identification

The radio-chromatograms of the 0–24 hours plasma, 0–48 hours urine, and 0–72 hours fecal samples are shown in Fig. 3. The identities of six proposed metabolites, including their biotransformation, elemental composition, protonated m/z ($[M + H]^+$) values (measured), mass error, and characteristic fragment ions, are summarized in Table 2. Table 3 lists the metabolites and their abundances as a percentage of the dose in urine, feces, and plasma. They are named by their molecular weight prefixed with “M,” except for the reference standard and its isomers.

Plasma. Two radio-chromatographic peaks were identified in the AUC-pooled 0–24 hours plasma (Fig. 3A). Unchanged HR011303 was the predominant drug-related component accounting for 87.93%, and M293 was a minor component constituting 3.46% of the total radioactivity in plasma.

M293. Metabolite M293 had a protonated molecular $[M + H]^+$ of m/z 293.9944 with a retention time of 28.02 minutes. The formula was C₁₃H₁₃NBrS based on the exact mass measurement, with the loss of CO₂ compared with HR011303. The major product ions of M293 were m/z 161.0291 and 239.9472 (Fig. 4, A and B), which were the same as those for HR011303. This suggested that M293 was a decarboxylated metabolite of HR011303.

Urine. Three radio-chromatographic peaks, including HR011303, were identified in the 0–48 hours pooled urine sample (Fig. 3B). HR011303 and two other abundant metabolites, M5 and M5/2, accounted for 4.62%, 51.57%, and 18.06% of the dose, respectively.

M5. The protonated molecular ion ($[M + H]^+$) of M5 was detected at m/z 514.0171. The formula was C₂₀H₂₁O₈NBrS based on the exact mass measurement. Comparison of the retention time and LC-MS/MS spectrum with the reference standard confirmed the structure as M5 (Fig. 4, C and D).

M5/2. M5/2 had a protonated molecular ion ($[M + H]^+$) of m/z 514.0160 (176.0315 Da greater than HR011303) and the same molecular weight as M5. The calculated elemental composition was C₂₀H₂₁O₈NBrS, indicating that M5/2 was generated through HR011303 glucuronidation. The product ions m/z 99.0442, 161.0293, 239.9472, and 337.9836 were the same as those of M5, implying that M5/2 and M5 were isomers (Fig. 4, E and F). The position of glucuronidation could not be confirmed using only MS data.

Feces. Four radio-chromatographic peaks were identified in the pooled 0–72 hours fecal samples (Fig. 3C). HR011303 and M424 were the two major drug-related components, accounting for 4.24% and 1.19% of the dose, respectively.

M424. M424 had a protonated molecular ion ($[M + H]^+$) of m/z 425.0167 (87.0322 Da greater than HR011303). The calculated elemental composition was C₁₇H₁₈O₄N₂BrS, an additional C₃H₅O₂N compared with HR011303. The formula indicated that M424 was generated through alanine conjugation and mono-oxidation. The main product

TABLE 3

Percent distribution of HR011303 and its metabolites in pooled plasma, urine and feces from human subjects

ID	Plasma %AUC	Urine		Feces		Urine+Feces
		81.50% of Dose		10.26% of Dose		91.75% of Dose
		%Urine	%Dose	%Feces	%Dose	%Dose
HR011303	87.93	5.67	4.62	41.86	4.24	8.86
M293	3.46	—	—	—	—	—
M394	—	—	—	6.81	0.69	0.69
M408	—	—	—	5.71	0.58	0.58
M424	—	—	—	11.73	1.19	1.19
M5	—	63.28	51.57	—	—	51.57
M5/2	—	22.16	18.06	—	—	18.06

%AUC derived from the proportion of 0–24 h pooled plasma; %Urine derived from the proportion of 0–48 h pooled urine; %Feces derived from the proportion of 0–72 h pooled feces; %Dose derived from the 0–216 h pooled urine and feces data; the proportion of 0–48 h pooled urine was 89.53% to total excretion rate of urine; the proportion of 0–72 h pooled feces was 73.88% to total excretion rate of feces; —, not detected.

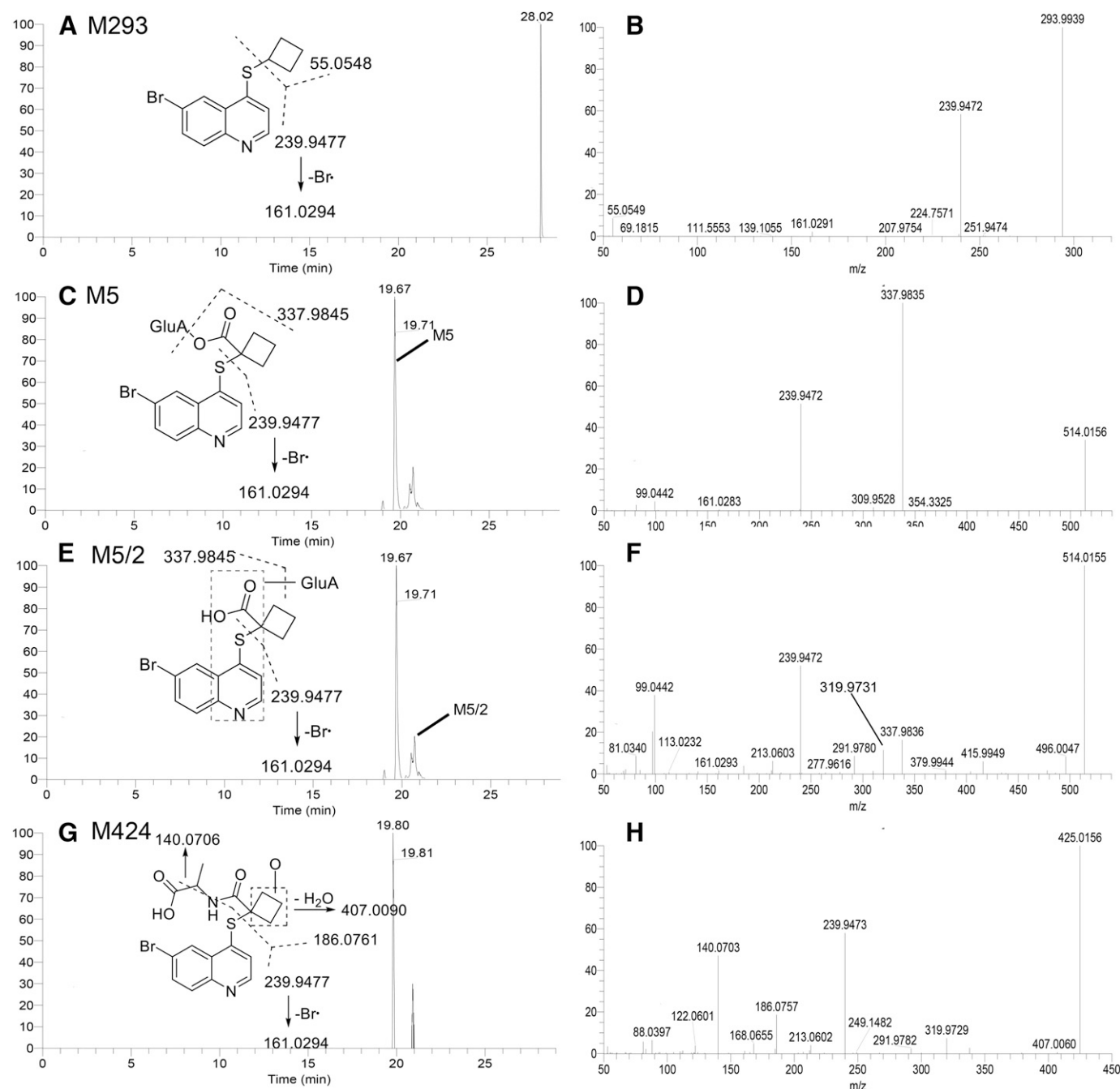


Fig. 4. Extracted ion chromatograms, product ion spectra, and proposed fragmentation patterns of M293 (A, B), M5 (C, D), M5/2 (E, F) and M424 (G, H).

ions were m/z 140.0703, 186.0757, 239.9473, 291.9782, and 319.9729, thus supporting the structure of M424 (Fig. 4, G and H).

M394 and M408, two metabolites derived from amino acid conjugation with HR011303, were also identified as minor metabolites in the pooled fecal sample.

The proposed metabolic pathway of HR011303 in healthy Chinese male subjects is shown in Fig. 5.

Screening by Recombinant UGTs

HR011303 was incubated with 13 human recombinant UGT isoforms individually in the presence of UDPGA. The formed metabolite M5 was identified by comparing the retention time and major product ions with the reference standard. Typical bar charts of the screening results

are shown in Fig. 6A. UGT1A3, UGT1A9, UGT2B4, and UGT2B7 catalyzed the formation of M5 with average formation rates of 20.93, 17.34, 15.12, and 82.36 pmol/min/mg protein, respectively. The other recombinant UGT enzymes showed almost no contribution to the metabolism of HR011303 to M5.

Chemical Inhibition Results

M5, the glucuronide metabolite, was identified after incubation of HR011303 with HLMs and HKMs in the presence of UDPGA, suggesting that liver and kidney microsomal enzymes participated in HR011303 glucuronidation. HR011303 glucuronidation in pooled HLMs was inhibited by fluconazole, indicating that UGT2B4 and UGT2B7 were involved in M5 formation. The inhibitory effects of niflumic acid and

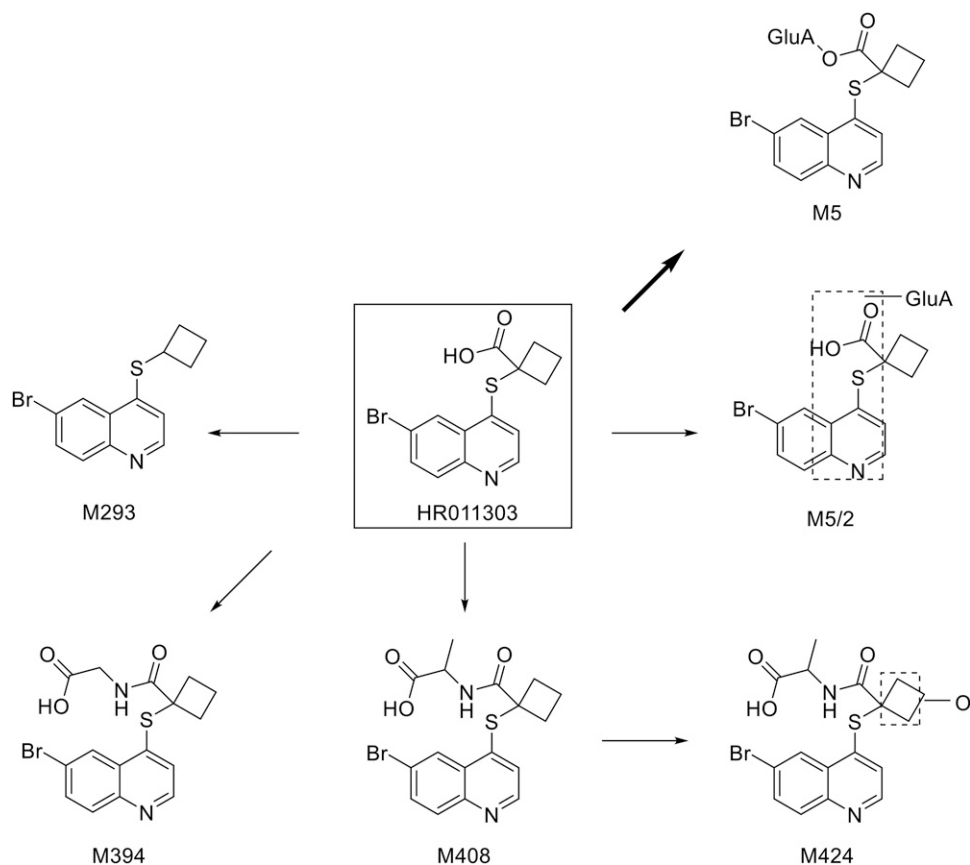


Fig. 5. Metabolic pathway of HR011303 in healthy Chinese male subjects.

fluconazole were also evaluated in pooled HKMs. The inhibitory effect of fluconazole on M5 formation mediated by UGT2B4/UGT2B7 in HLMs (35% decrease) or HKMs (25% decrease) was moderate at a high concentration (2.5 mM) but minimal at 1 mM in HLMs (20% decrease) or HKMs (13% decrease) as shown in Fig. 6B. The inhibitory effect of niflumic acid, a specific UGT1A9 inhibitor, was minor at a concentration of 25 μM in HKMs (13% decrease) and nonexistent at 2.5 μM as shown in Fig. 6C.

Kinetics of HR011303 Glucuronidation by r-UGTs

As noted above, since UGT2B4 and UGT2B7 were the two major enzymes responsible for M5 formation, kinetics studies were performed to assess their contribution in catalyzing M5 formation. The profiles are presented in Fig. 7. The kinetics profile of UGT2B4 matched the biphasic kinetic model (Fig. 7A). UGT2B4 showed high affinity activity with a K_{m1} of 56.5 μM and an intrinsic clearance (CL_{int}) of 10.9 $\mu\text{L}/\text{min}/\text{mg}$ protein, and also low affinity activity with a K_{m2} value that was not calculated. Additionally, the kinetics profile of UGT2B7 was fitted to the substrate inhibition model (Fig. 7B). The K_m , dissociation constant, V_{max} and CL_{int} values were 3.6 μM , 140.3 μM , 4142.0 $\text{pmol}/\text{min}/\text{mg}$ protein, and 1156.0 $\mu\text{L}/\text{min}/\text{mg}$ protein, respectively.

Discussion

This study presents the pharmacokinetics, mass balance, and metabolism of [^{14}C]HR011303 in six healthy Chinese male subjects. At 216 hours postdose, 91.75% of the administered radioactivity was recovered in the urine (81.50%) and feces (10.26%), indicating complete excretion. Most of the administered radioactivity was recovered within

96 hours after dosing, with 79.89% in the urine and 9.50% in the feces. The mass balance results indicated that renal excretion was the predominant elimination route for the HR011303 drug-related components, which was quite opposite to that displayed in rats (companion manuscript, DMD-AR-2021-000582). The difference in the excretion pathways between humans and rats indicates that species differences in the excretion pattern can be possible.

Amino acid conjugation is an important phase II metabolic pathway (Mizuno et al., 2019). In this study, three amino acid conjugation metabolites (including two alanine conjugates and one glycine conjugate) were deduced from feces based on their full MS and tandem mass spectrometry spectra. However, their structures were not confirmed since reference standards are not available. Although the formation of glycine conjugates of carboxylic acids is a known metabolic pathway, the formation of alanine conjugates has rarely been observed. For instance, Wallcave et al. reported the formation of an alanine conjugate of 4,4'-dichlorophenylacetic acid in mouse (Wallcave et al., 1974). Additionally, the excretion of amino acid conjugates via the feces has rarely been reported. One possible pathway for the formation of these conjugates is by gut bacteria (Feng et al., 2019). Recent research has reported that gut microbiota are able to catalyze phenylalanine and leucine conjugation to the carboxyl position of bile acids (Guzior and Quinn., 2021). Thus, one can speculate that amino acid conjugates, specifically alanine conjugation caused by gut bacteria, may be possible. However, this hypothesis requires further investigation.

As mentioned previously, M293 was identified in human plasma as the decarboxylated metabolite of HR011303, even though its reference standard was not obtained. HR011303 contains a quinoline ring, which always undergoes decarboxylation (Dalvie et al., 2008;

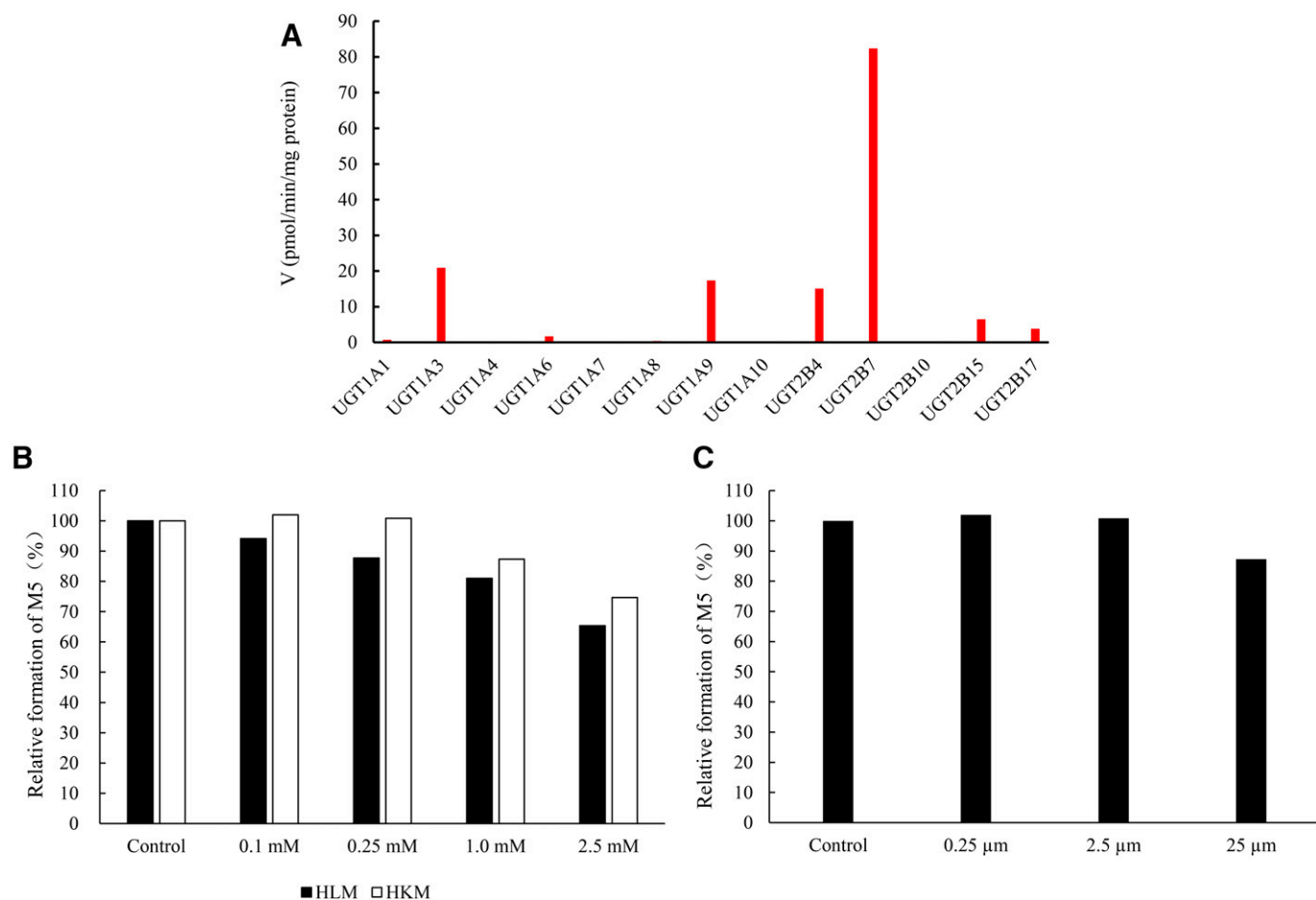


Fig. 6. M5 formation rate after incubation of HR011303 with human recombinant UGT (A); relative formation of M5 after incubation of HR011303 with fluconazole in HLMs or HKMs (B); relative formation of M5 after incubation of HR011303 with niflumic acid in HKMs (C).

Bershas et al., 2013). The proposed formation mechanism of M293 is shown in Fig. 8. The nitrogen of the quinoline in HR011303 serves as a Lewis base to take the proton from another HR011303 molecule; subsequently, the protonated carboxylic acid could be decarboxylated via an intermolecular cyclic transition state. Furthermore, the Br atom on the quinoline ring, acting as an electron-withdrawing substituent, could further facilitate carbon-carbon bond cleavage (Dalvie et al., 2008).

UGTs are a family of conjugation enzymes that play important roles in the metabolism and detoxification of many drugs (Court et al., 2012; Rowland et al., 2013; Oda et al., 2015). In this study, UGT2B4 and UGT2B7 were the main UGT informs responsible for HR011303 glucuronidation. As observed from the enzyme kinetics studies, HR011303 glucuronidation exhibited substrate inhibition for UGT2B7 (Fig. 7A), which did not obey typical Michaelis-Menten kinetics models. Substrate inhibition kinetics imply that there are two substrate binding sites within each enzyme subunit: one site catalyzes the substrate, whereas the other site reduces the rate of reaction after substrate binding (Leow and Chan, 2019). UGT2B4 displayed another atypical Michaelis-Menten kinetics model during HR011303 glucuronidation, i.e., biphasic kinetics (Fig. 7B). Biphasic kinetics was readily observed in heterogeneous systems such as HLMs and the human liver S9 fraction, where more than one enzyme are involved. However, biphasic kinetics has also been reported for recombinant enzymes (Wei et al., 2007). Although CL_{int} values calculated by dividing V_{max} by K_m better fit typical Michaelis-Menten kinetics, the formula applied to obtain the CL_{int} values for atypical

Michaelis-Menten kinetics models was also reported (Ma et al., 2007). In this study, we calculated the CL_{int} values for UGT2B7 and UGT2B4 in this way, and these estimated CL_{int} values of 1,156.0 and 10.9 μ L/min/mg protein for UGT2B7 and UGT2B4 suggested that UGT2B7 was the predominant enzyme that catalyzed HR011303 glucuronidation.

Urine excretion was the predominant excretion route of HR011303, accounting for 81.50% of the administered dose. Therefore, we focused on the main metabolites in urine, i.e., M5 (51.57% of the dose) and M5/2 (18.06% of the dose). The stability of M5 in PBS at pH 7.57 was evaluated, and the $t_{1/2}$ of M5 was 4.58 hours, which is longer than the indicator of chemical stability (3.6 hours) (Sawamura et al., 2010), suggesting that M5 was moderately stable in PBS. M5 stability in plasma at 0°C and 37°C was also evaluated, and the results revealed that M5 was stable in plasma at 0°C in the presence of protease inhibitor cocktail but unstable at 37°C. In addition, we evaluated the stability of M5 in human urine, and the results showed that M5 was stable in human urine for at least 1 hour at 37°C, which is longer than the urine collection time in the clinical facility. Based on the results from the HLMs/HKMs incubations and M5 stability in PBS, plasma, and urine, we speculated that M5 is generated by hepatocytes, subsequently hydrolyzed to HR011303 in plasma, once again metabolized to M5 in the kidney, and finally excreted in the urine. The PBS incubation samples were also subjected to liquid chromatography-high resolution mass spectrometry for analysis, and approximately 7% of M5 transformed to M5/2 after incubation for 60 minutes. M5/2 is most

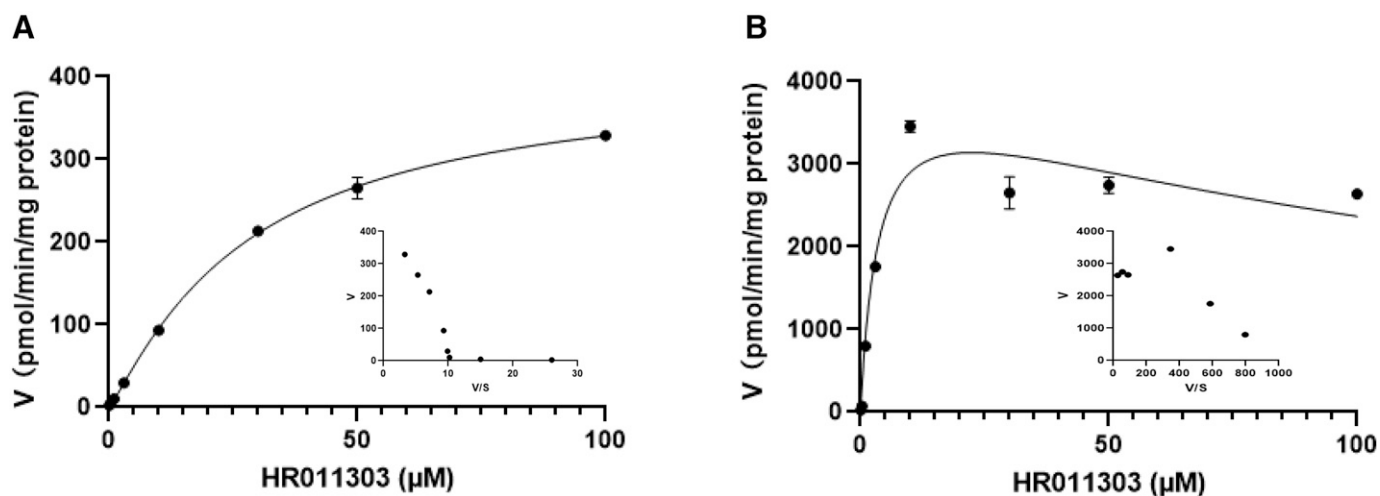


Fig. 7. Kinetics profiles for the formation of HR011303 glucuronide catalyzed by UGT2B4 (A) and UGT2B7 (B). Inset, Eadie-Hofstee plots for each of the profiles are shown.

likely the result of acyl migration of M5, which is associated with acyl glucuronide reactivity. Acyl glucuronide intermediates are potential reactive intermediates that may cause unexpected side effects (Boelsterli 2002; Bradshaw et al., 2020), although no abnormal clinical significance or adverse events occurred in the current clinical trial.

In conclusion, this study explored the absorption, metabolism, and excretion of HR011303 in humans. Treatment with a single dose of 10 mg of [^{14}C]HR011303 (80 μCi) is safe and well tolerated by healthy male subjects. Mass balance analysis revealed that 91.75% of the dose was recovered in urine (81.50%) and feces (10.26%) after oral administration. M5, a glucuronide metabolite of HR011303, was the major

metabolite of HR011303, accounting for 51.57% of the dose. In vitro studies identified UGT2B7 in HLMs as the major UGT responsible for M5 formation.

Authorship Contributions

Participated in research design: Zheng, H. Zhang, Li, Z. Zhang, Lin, Zhong, Miao, Diao.

Conducted experiments: Zheng, Liu.

Contributed new reagents or analytic tools: H. Zhang, Ma, Miao.

Performed data analysis: Zheng, Liu, H. Zhang, Zhan, Chen, Diao.

Wrote or contributed to the writing of the manuscript: Zheng, H. Zhang, Zhong, Miao, Diao.

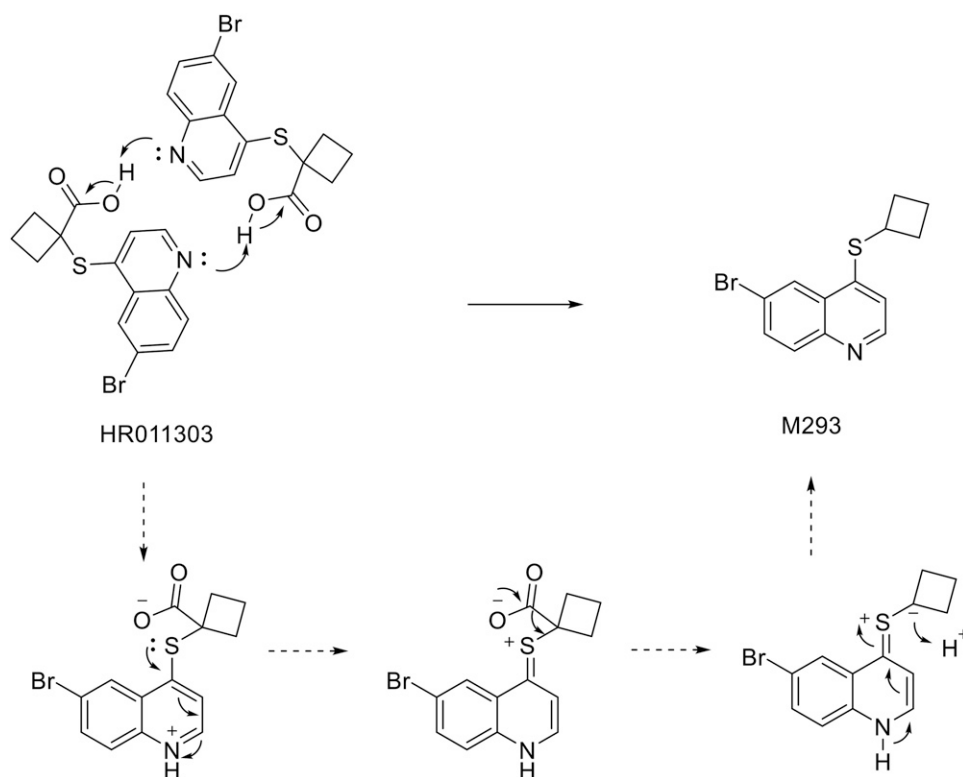


Fig. 8. The proposed formation pathway of M293.

References

- Al Saabi A, Allorge D, Sauvage FL, Tournel G, Gaulier JM, Marquet P, and Picard N (2013) Involvement of UDP-glucuronosyltransferases UGT1A9 and UGT2B7 in ethanol glucuronidation, and interactions with common drugs of abuse. *Drug Metab Dispos* **41**:568–574.
- Bershas DA, Ouellet D, Mamari-Fishman DB, Nebot N, Carson SW, Blackman SC, Morrison RA, Adams JL, Jurusik KE, Knecht DM, et al. (2013) Metabolism and disposition of oral dabrafenib in cancer patients: proposed participation of aryl nitrogen in carbon-carbon bond cleavage via decarboxylation following enzymatic oxidation. *Drug Metab Dispos* **41**:2215–2224.
- Bian YC, Zhang H, Ma S, Jiao YY, Yan PK, Liu X, Ma SP, Xiong YT, Gu ZM, Yu ZW, et al. (2021) Mass balance, pharmacokinetics and pharmacodynamics of intravenous HSK3486, a novel anaesthetic, administered to healthy subjects. *Br J Clin Pharmacol* **87**:93–105. 10.1111/bcp.14363.
- Boelsterli UA (2002) Xenobiotic acyl glucuronides and acyl CoA thioesters as protein-reactive metabolites with the potential to cause idiosyncratic drug reactions. *Curr Drug Metab* **3**:439–450.
- Bradshaw PR, Athersuch TJ, Stachulski AV, and Wilson ID (2020) Acyl glucuronide reactivity in perspective. *Drug Discov Today* **25**:1639–1650.
- Burns CM and Wortmann RL (2011) Gout therapeutics: new drugs for an old disease. *Lancet* **377**:165–177.
- Court MH, Zhang X, Ding X, Yee KK, Hesse LM, and Finel M (2012) Quantitative distribution of mRNAs encoding the 19 human UDP-glucuronosyltransferase enzymes in 26 adult and 3 fetal tissues. *Xenobiotica* **42**:266–277.
- Dalvie D, Chen W, Zhang C, Vaz AD, Smolarek TA, Cox LM, Lin J, and Obach RS (2008) Pharmacokinetics, metabolism, and excretion of torcetrapib, a cholesterol ester transfer protein inhibitor, in humans. *Drug Metab Dispos* **36**:2185–2198.
- Dong Y, Zhao T, Ai W, Zalloum WA, Kang D, Wu T, Liu X, and Zhan P (2019) Novel urate transporter 1 (URAT1) inhibitors: a review of recent patent literature (2016–2019). *Expert Opin Ther Pat* **29**:871–879.
- Feng YL, Cao G, Chen DQ, Vaziri ND, Chen L, Zhang J, Wang M, Guo Y, and Zhao YY (2019) Microbiome-metabolomics reveals gut microbiota associated with glycine-conjugated metabolites and polyamine metabolism in chronic kidney disease. *Cell Mol Life Sci* **366**:4961–4978.
- Gliozzi M, Malara N, Muscoli S, and Mollace V (2016) The treatment of hyperuricemia. *Int J Cardiol* **213**:23–27.
- Guzior DV and Quinn RA (2021) Review: microbial transformations of human bile acids. *Microbiome* **9**:140.
- Hediger MA, Johnson RJ, Miyazaki H, and Endou H (2005) Molecular physiology of urate transport. *Physiology (Bethesda)* **20**:125–133.
- Hop CE, Wang Z, Chen Q, and Kwei G (1998) Plasma-pooling methods to increase throughput for in vivo pharmacokinetic screening. *J Pharm Sci* **87**:901–903.
- Hoy SM (2016) Lesinurad: first global approval. *Drugs* **76**:509–516.
- Hutzler JM and Tracy TS (2002) Atypical kinetic profiles in drug metabolism reactions. *Drug Metab Dispos* **30**:355–362.
- Hyndman D, Liu S, and Miner JN (2016) Urate handling in the human body. *Curr Rheumatol Rep* **18**:34–42.
- Jordan A and Gresser U (2018) Side effects and interactions of the xanthine oxidase inhibitor febuxostat. *Pharmaceuticals (Basel)* **11**:51–70.
- Kuo CF, Grainge MJ, Zhang W, and Doherty M (2015) Global epidemiology of gout: prevalence, incidence and risk factors. *Nat Rev Rheumatol* **11**:649–662.
- Kuo TM, Huang CM, Tu HP, Min-Shan Ko A, Wang SJ, Lee CP, and Ko YC (2017) URAT1 inhibition by ALPK1 is associated with uric acid homeostasis. *Rheumatology (Oxford)* **56**:654–659.
- Lee JM, Kim HC, Cho HM, Oh SM, Choi DP, and Suh I (2012) Association between serum uric acid level and metabolic syndrome. *J Prev Med Public Health* **45**:181–187.
- Leow JWH and Chan EY (2019) Atypical Michaelis-Menten kinetics in cytochrome P450 enzymes: a focus on substrate inhibition. *Biochem Pharmacol* **169**:113615.
- Lipsky PE, Calabrese LH, Kavanaugh A, Sundy JS, Wright D, Wolfson M, and Becker MA (2014) Pegloticase immunogenicity: the relationship between efficacy and antibody development in patients treated for refractory chronic gout. *Arthritis Res Ther* **16**:R60.
- Liu H, Zhang XM, Wang YL, and Liu BC (2014) Prevalence of hyperuricemia among Chinese adults: a national cross-sectional survey using multistage, stratified sampling. *J Nephrol* **27**:653–658.
- Ma B, Polsky-Fisher SL, Vickers S, Cui D, and Rodrigues AD (2007) Cytochrome P450 3A-dependent metabolism of a potent and selective gamma-aminobutyric acid A α 2/3 receptor agonist in vitro: involvement of cytochrome P450 3A5 displaying biphasic kinetics. *Drug Metab Dispos* **35**:1301–1307.
- Maiuolo J, Oppedisano F, Gratteri S, Muscoli C, and Mollace V (2016) Regulation of uric acid metabolism and excretion. *Int J Cardiol* **213**:8–14.
- Mizuno K, Takeuchi K, Umehara K, and Nakajima M (2019) Identification of novel metabolites of vildagliptin in rats: thiazoline-containing thiol adducts formed via cysteine or glutathione conjugation. *Drug Metab Dispos* **47**:809–817.
- Novikov A, Fu Y, Huang W, Freeman B, Patel R, van Ginkel C, Koepsell H, Busslinger M, Onishi A, Nespoux J, et al. (2019) SGLT2 inhibition and renal urate excretion: role of luminal glucose, GLUT9, and URAT1. *Am J Physiol Renal Physiol* **316**:F173–F185.
- Oda S, Fukami T, Yokoi T, and Nakajima M (2015) A comprehensive review of UDP-glucuronosyltransferase and esterases for drug development. *Drug Metab Pharmacokinet* **30**:30–51.
- Pacher P, Nivorozhkin A, and Szabó C (2006) Therapeutic effects of xanthine oxidase inhibitors: renaissance half a century after the discovery of allopurinol. *Pharmacol Rev* **58**:87–114.
- Peng J, Hu Q, Gu C, Liu B, Jin F, Yuan J, Feng J, Zhang L, Lan J, Dong Q, et al. (2016) Discovery of potent and orally bioavailable inhibitors of human uric acid transporter 1 (hURAT1) and binding mode prediction using homology model. *Bioorg Med Chem Lett* **26**:277–282.
- Punzi L, Scanu A, Ramonda R, and Oliviero F (2012) Gout as autoimmune disease: new mechanisms for more appropriated treatment targets. *Autoimmun Rev* **12**:66–71.
- Ramírez J, Mirkov S, House LK, and Ratain MJ (2015) Glucuronidation of OTS167 in humans is catalyzed by UDP-glucuronosyltransferases UGT1A1, UGT1A3, UGT1A8, and UGT1A10. *Drug Metab Dispos* **43**:928–935.
- Richette P and Bardin T (2010) Gout. *Lancet* **375**:318–328.
- Rowland A, Miners JO, and Mackenzie PI (2013) The UDP-glucuronosyltransferases: their role in drug metabolism and detoxification. *Int J Biochem Cell Biol* **45**:1121–1132.
- Sakiyama M, Matsuo H, Shimizu S, Nakashima H, Nakamura T, Nakayama A, Higashino T, Naito M, Suma S, Hishida A, et al. (2016) The effects of URAT1/SLC22A12 nonfunctional variants, R90H and W258X, on serum uric acid levels and gout/hyperuricemia progression. *Sci Rep* **6**:20148.
- Sawamura R, Okudaira N, Watanabe K, Murai T, Kobayashi Y, Tachibana M, Ohnuki T, Masuda K, Honma H, Kurihara A, et al. (2010) Predictability of idiosyncratic drug toxicity risk for carboxylic acid-containing drugs based on the chemical stability of acyl glucuronide. *Drug Metab Dispos* **38**:1857–1864.
- Sui X, Church TS, Meriwether RA, Lobelo F, and Blair SN (2008) Uric acid and the development of metabolic syndrome in women and men. *Metabolism* **57**:845–852.
- Tian H, Liu W, Zhou Z, Shang Q, Liu Y, Xie Y, Liu C, Xu W, Tang L, Wang J, et al. (2016) Discovery of a flexible triazolylbutanoic acid as a highly potent uric acid transporter 1 (URAT1) inhibitor. *Molecules* **21**:1543.
- Wallace L, Bronczyk S, and Gingell R (1974) Excreted metabolites of 1,1,1-trichloro-2,2-bis(p-chlorophenyl)ethane in the mouse and hamster. *J Agric Food Chem* **22**:904–908.
- Wang J, Yao W, Fan D, Qiu Z, Song J, Pan K, and Hang T (2019) An LC-MS/MS method for quantification of HR011303, a novel highly selective urate transporter 1 inhibitor in beagle dogs and the application to a pharmacokinetic study. *Biomed Chromatogr* **33**:e4604.
- Wei L, Lococus CW, and Tracy TS (2007) Polymorphic variants of CYP2C9: mechanisms involved in reduced catalytic activity. *Mol Pharmacol* **72**:1280–1288.
- Zheng YD, Zhang H, Zhan Y, Bian YC, Ma S, Gan HX, Lai XJ, Liu YQ, Gong YC, Liu XF, et al. (2021) Pharmacokinetics, mass balance, and metabolism of [14 C]vicagrel, a novel irreversible P2Y $_{12}$ inhibitor in humans. *Acta Pharmacol Sin* **42**:1535–1546.
- Zoccali C and Mallamaci F (2013) Uric acid, hypertension, and cardiovascular and renal complications. *Curr Hypertens Rep* **15**:531–537.

Address correspondence to: Dr. Xingxing Diao, Shanghai Institute of Materia Medica, Chinese Academy of Sciences, 501 Haik Road, Zhangjiang Hi-Tech Park, Shanghai, China, 201210. E-mail: xxdiao@simm.ac.cn